LA-UR-81-2530

MASTER

CONF-810845--3

Los Alamos National Laboratory is operated by the University of California for the United States Department of Energy under contract W-7405-ENG-36

TITLE Measurement of Gas Density and Temperature Distributions in Strongly Rotating UF_6 Using Laser-Induced Fluorescence

AUTHOR(S) Richard A. Gentry
Stephen E. Caldwell
Ralph W. White

SUBMITTED TO To be presented at the 4th Workshop on Gases in Strong Rotation, Oxford, England, Aug. 24-27, 1981.

Los Alamos National Laboratory
Los Alamos, New Mexico 87545

ABSTRACT

A new technique for using Laser Induced Fluorescence (LIF) signals to measure the distribution of gas density and temperature in strongly rotating UF_6 gas is presented. An external pulsed laser is used to excite the rotating UF_6 gas, producing an exponentially decaying fluorescence signal.

A multi-channel fiber optics system simultaneously collects the fluorescence signals emanating from a number of points in the gas. The signals from each optical channel are digitized and processed to determine the fluorescence signal intensity and decay lifetime at each of the points of observation by means of a least squares fitting process. Gas densities and temperatures are then determined from the intensity and lifetime data.

A recently constructed LIF probe system is described and an analysis of the unfolding techniques necessary to process the signal data is presented. Preliminary data, obtained in tests of the probe system in a laboratory rotor, are presented.

INTRODUCTION

Recently there has been interest expressed in using laser induced fluorescence (LIF) as a realtime diagnostic technique for measuring UF_6 pressures in uranium isotope processing streams.[1-2] Work by Rice et al.[3] has shown that the LIF quenching lifetime is a unique, sensitive function of pressure and temperature in a broad range of gas conditions. Also, the fluorescence intensity is essentially proportional to the gas density. Thus, the LIF signal can be unfolded to obtain information describing both the UF_6 temperature and number density. An experimental program is in progress at the Los Alamos National Laboratory to develop and test an LIF probe to measure radial distributions of UF_6 gas density and temperature in a highly stratified, confined rotating gas flow similar to those experienced in a gas centrifuge. Some encouraging results have been obtained in testing a prototype LIF probe in a UF_6 gas filled laboratory rotor. A description of the LIF probe, an analysis of the operating characteristics of the probe, and some preliminary data obtained in recent experiments will be presented in following sections.

OVERVIEW

When gaseous UF_6 is excited by a pulsed dye laser in the long wavelength region of the $A-\tilde{X}$ band ($\lambda > 360$ nm), laser induced fluorescence is observed. The observed fluorescence exhibits a peak emission wavelength near 421 nm[4]. Time-resolved measurements of the LIF emission in UF_6 by Benetti et al.[5] showed that the fluorescence emission history occurs in two phases. The first phase consists of a rapidly decaying transient fluorescence pulse that has a duration on the order of 1 ns. This transient phase is immediately followed by a lower amplitude, exponentially decaying phase that is characterized by a much longer decay lifetime. The decay lifetime of the second, long lived fluorescence phase is strongly dependent on the gas temperature and pressure. It is the information that is contained in the second phase of the fluorescence emission process that is of interest here. In the following work we will be referring to the signal characteristics of the second phase of the LIF fluorescence.

Oldenborg et al. have shown that the shape of the room temperature UF_6 LIF spectrum is essentially independent of the excitation wavelength in the wavelength region of interest here.[4] In the same work, they have also shown that the shape of the LIF emission spectrum is independent of the gas pressure at pressures ranging from 0.2 torr to 20.0 torr. From this we conclude that the spectral characteristics of the observed LIF signal are not likely to vary greatly with changes in gas conditions at the point of excitation.

Only a small fraction of the initially excited UF_6 molecules eventually fluoresce; i.e., the fluorescence quantum efficiency* is very small ($\lesssim 10^{-3}$). The reason for this is that an excited molecule can follow a number of de-excitation paths; however, only a small fraction of the molecules eventually traverse a de-excitation path that leads to the emission of a fluorescence photon. The generally accepted explanation of the excitation-fluorescence process occurring is illustrated in Figure 1.[4] Figure 1 is an energy diagram illustrating the ground state and the low lying energy states involved in the LIF process. The UF_6 molecules that absorb photons are initially excited into the higher energy states A_1' and A_2. These states are coupled through bi-molecular collisions to a lower lying excited energy state A_1. The long lived LIF signal is produced when molecules in the A_1 state emit photons as they return to the ground state. The fluorescence photon flux is proportional to the number of molecules in the A_1 state in the radiating volume element. The A_1 state is depopulated by: (1) fluorescence or (2) dissociation of the molecule, which is dependent upon the intermolecular collision rate.

---

*The fluorescence quantum effiency is the fraction of the initially excited molecules that eventually fluoresce.

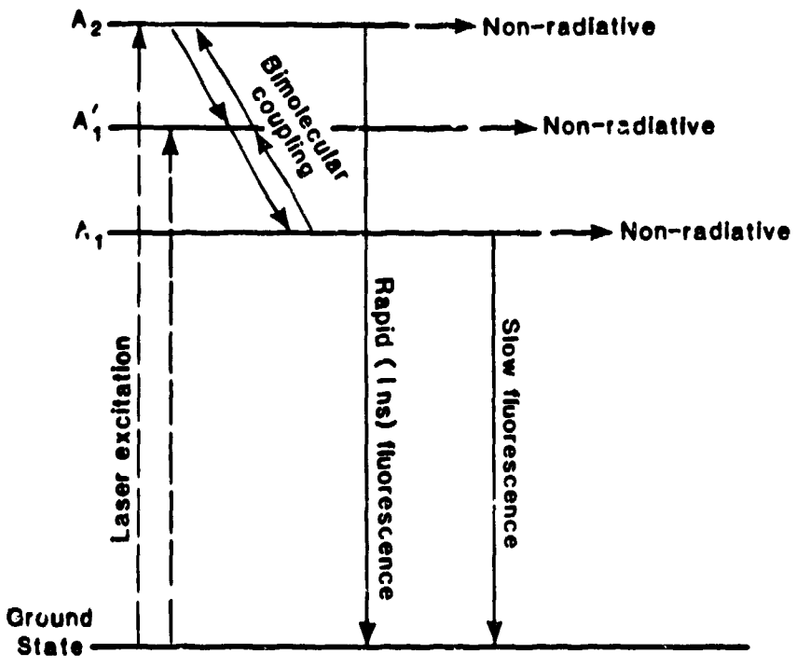

Figure 1. Energy diagram illustrating coupling of UF_6 excited states involved in the LIF process

Since the fluorescence photon flux history depends upon the molecular collision rate, both the LIF decay lifetime and the LIF signal intensity depend on the gasdynamic parameters that determine the molecular collision rate, the gas density and temperature. The LIF signal, then, contains two types of information:

1. The signal intensity, which is essentially determined by the average UF_6 gas number density.
2. The LIF decay lifetime, which contains information relating to the average collision rate between UF_6 molecules in the radiating volume element. The decay lifetime is a function of both the gas density and temperature (or, equivalently a function of the gas pressure and temperature).

The variation of the fluorescence decay lifetime with gas pressure and temperature is shown in Figure 2. Fluorescence lifetime is plotted here as a function of gas pressure for three temperatures, 20° C, 40° C and 60° C. The data shown here was obtained by Rice et al.[3,6] The solid curves are obtained from a fluorescence lifetime model developed by Rice et al. to fit their data.[3]

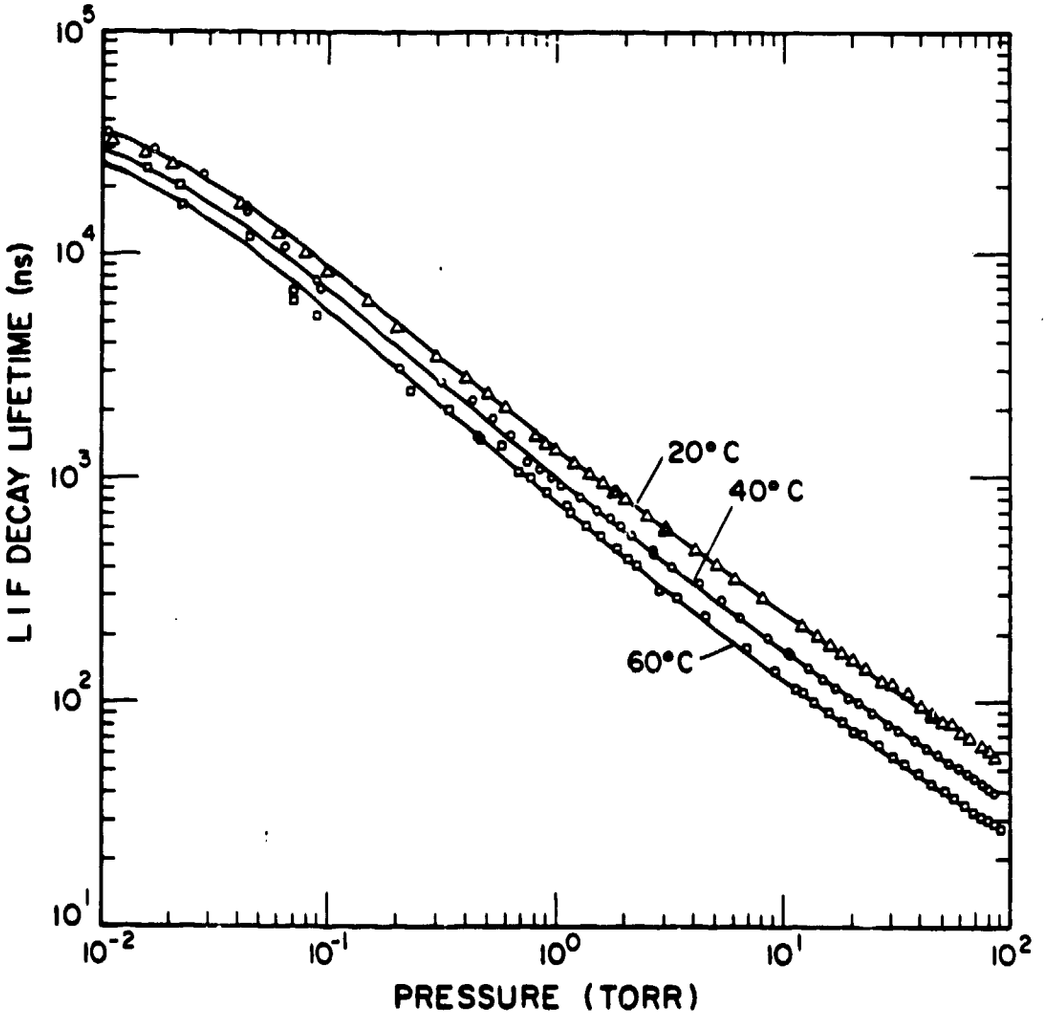

Figure 2. UF_6 LIF decay lifetime vs gas pressure at various gas temperatures. (Rice et al.)[3,6]

Several things can be seen here:

1. At a given gas pressure, the lifetime decreases with increasing gas temperature.
2. At a given gas temperature, the lifetime decreases with increasing gas pressure.
3. At a given gas pressure, the lifetime is quite sensitive to the gas temperature, particularly at higher gas pressures. At a gas temperature and pressure of 40° C and 80 torr respectively, for example, a 1° C change in gas temperature causes a decay lifetime change of approximately 2%.
4. The lifetime is a unique function of gas pressure and temperature in the regime where lifetime measurements have been made.
5. There is a very large variation in the lifetime over pressure ranges of interest. Lifetimes vary from tens of nanoseconds to tens of microseconds as the pressure varies from 100 torr to 10^{-2} torr. Thus, LIF measurement techniques must involve the acquisition and processing of signal data with widely varying lifetimes.

As the UF_6 gas pressure decreases, the fluorescence quantum efficiency rises. Thus, the integrated LIF signal decreases relatively slowly with gas pressure. As a result, the LIF measurement process is characterized by a relatively large dynamic range. This is important for probing highly stratified, strongly rotating UF_6 flows.

The trace of a typical LIF signal is shown in Figure 3. The initial higher amplitude spike is caused by the scattered light from the laser excitation pulse, which is far more intense than the actual fluorescence signal. The later, exponentially decaying portion of the trace is the actual fluorescence signal, visible after the laser pulse has been extinguished. The fluctuations visible are primarily caused by two effects:

1. Photon fluctuation effects.
2. Noise effects.

In order to analyze the signal, the signal is sampled over a number of sampling periods in the time period following extinguishment of the laser pulse. The average signal intensity in each sampling period is determined by integrating the photomultiplier tube current over the sampling period (t_k to $t_k + \Delta t_k$). Signal intensity information is summed over a number of laser pulses to reduce the effects of noise and photon fluctuation effects and to obtain data relating to the statistical quality of the signal. Finally, the signal intensity and decay lifetime are determined by least square fitting techniques.

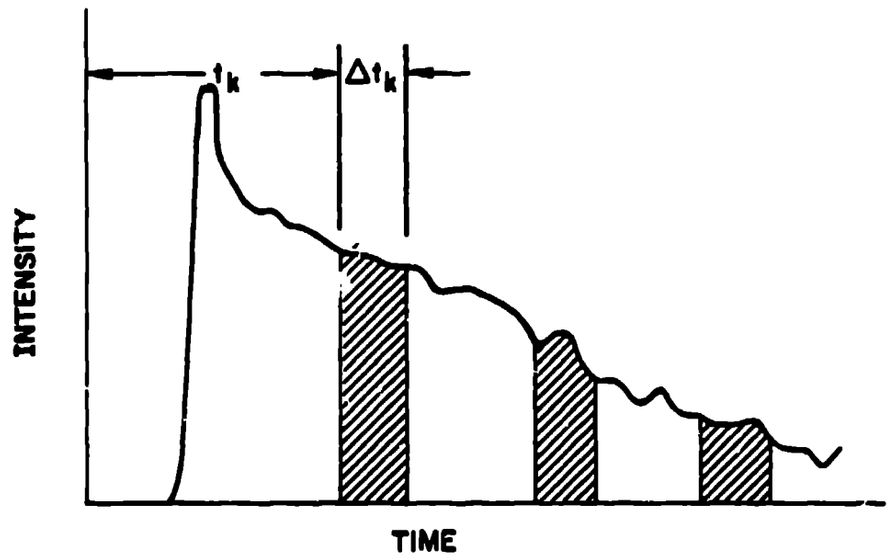

Fig. 3. Trace of a typical LIF signal

LIF PROBE OPTICAL SYSTEM

A schematic diagram of the LIF probe is shown in Figure 4. An externally produced 392.1 nm laser beam is directed into the gas layer near the rotor wall and the resulting fluorescence light is transmitted to photomultiplier tubes located outside the rotor. All internal optical system components are positioned in the vacuum core, far from the rotor wall, in order to avoid disturbing the gas flow.

The laser is a Quanta-Ray YAG pumped dye laser operating at 10 Hz, 1 mj/pulse, and 15 ns pulse width. The beam is focused to a diameter of approximately 2 mm in the gas layer. Approximately 0.1% of the UF_6 molecules within the beam path are excited with each laser pulse. The fluorescence decay lifetime ranges from 40 μs in the zero pressure limit to about 40 ns at a pressure of 100 torr; therefore, all decay measurements can be made after the 15 ns laser pulse has been extinguished.

Three internal mirrors direct the laser beam toward the rotor wall, causing the beam to intersect the wall at an angle of 55° to the normal. Excited UF_6 molecules form a line source of fluorescent light. A telescope produces an image of the fluorescing gas on the face of a fiber optics bundle, located near the axis of the rotor. The telescope consists of two lenses (42 mm diameter x 150 mm focal length) and two broad band filters that pass the fluorescence band (400-440 nm) and reject scattered laser light (392.1 nm).

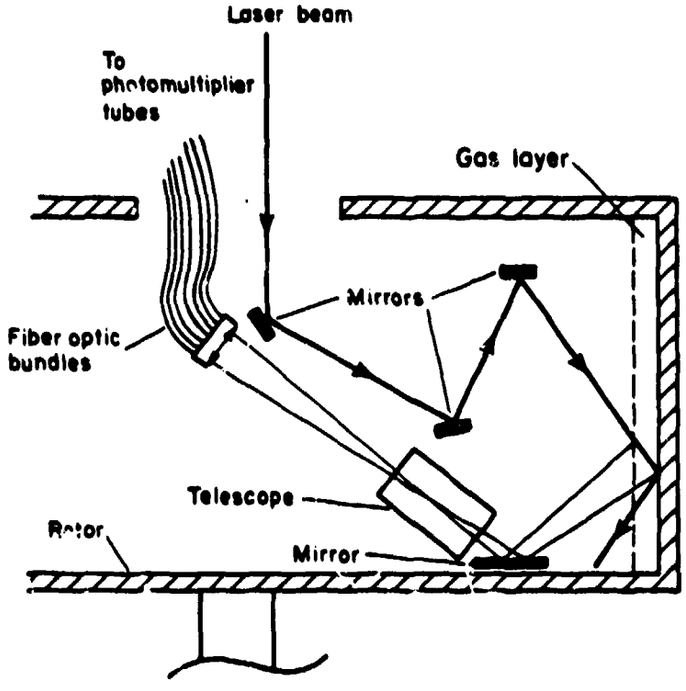

Figure 4. Schematic diagram illustrating the internal optical components of the LIF probe system.

The fiber optics bundle dissects the fluorescence image into 26 parts (see Figure 5), representing 26 radial locations of fluorescing gas. The light from each of the 26 sub-images is carried via its own incoherent fiber bundle to an externally mounted RCA 4837 photomultiplier tube.

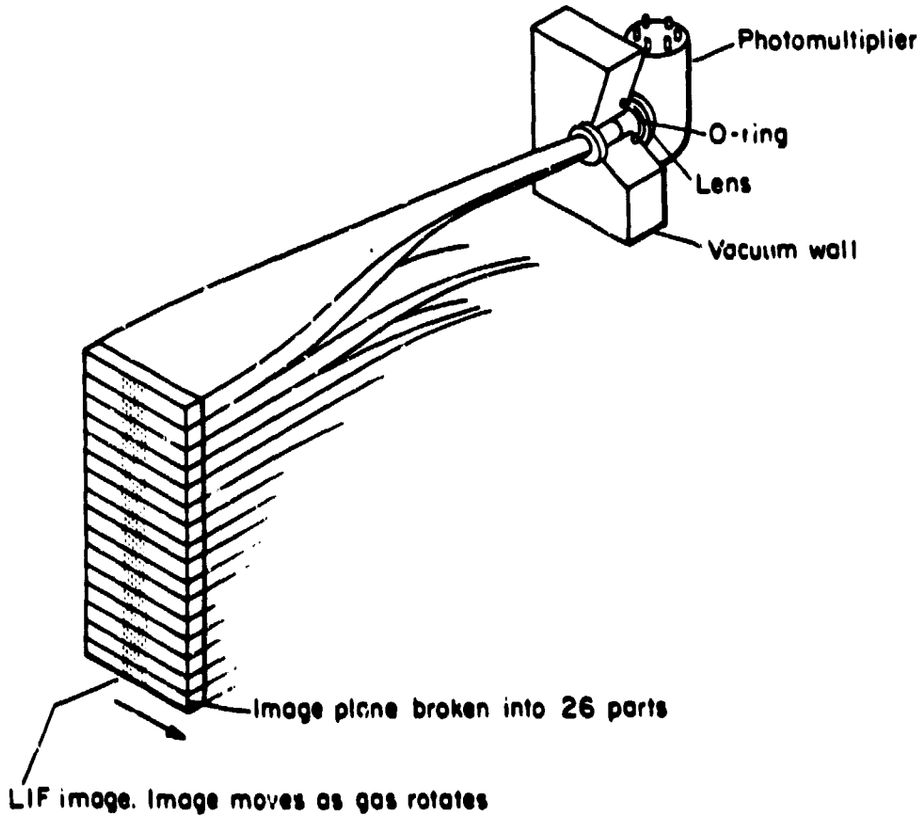

Figure 5. Schematic diagram illustrating optical dissection of the LIF image

Photographs of the major components of the probe optical system are shown in Figures 6 through 9. Figure 6 is a photograph of the mirror system used to direct the incoming laser beam to the gas layer near the rotor wall. Two of the three mirrors are adjustable. The guiding mirrors are mounted on a rigid arm that is fastened to a mounting ring, which fastens to the external rotor cover plate. Figure 7 is a photograph of the mirror, telescope and fiber bundles used to detect the LIF signal. The telescope and mirror are also fastened to a rigid arm that is fastened to a mounting ring. These two subassemblies of the interior optical system have mounting rings with matching sets of pins and alignment holes to insure that when they are bolted to the rotor cover plate they are properly aligned. Figure 8 is a photograph showing the beam mirror system and telescope fastened together on an external holding jig. The incoming vertical laser beam is reflected from mirror (1) to mirror (2) to mirror (3), which aligns the beam to the desired wall incidence angle. The LIF signal is reflected by mirror (4), causing the LIF signal to enter the telescope. The optical fiber system that views the telescope image plane is visible at the top of the photograph. Figure 9 is a photograph of the external optical housing used to handle the incoming and outgoing beams. The incoming laser beam is directed into the rotor by the movable mirror mounted on the optical post (1). The incoming beam enters through the window (2), which is titled at an angle of 10° with respect to the beam. A small fraction of the laser beam incident at the window is reflected into the beam monitoring detector (3), which

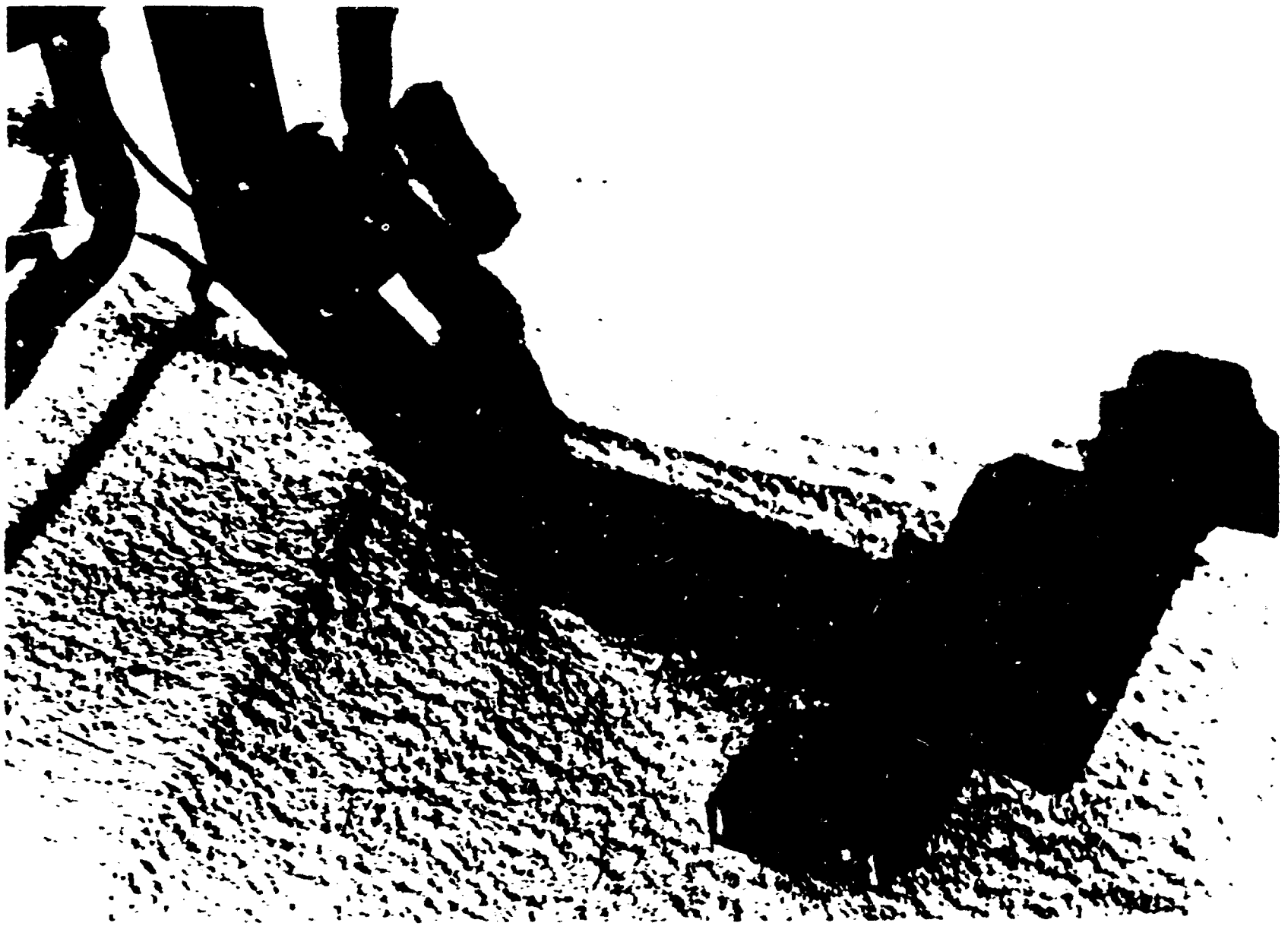

Figure 6. Photograph of the mirror system used to guide the incoming laser beam to the rotor wall

Figure 7. Photograph of the mirror, telescope and fiber optics bundle used to view the LIF signal.

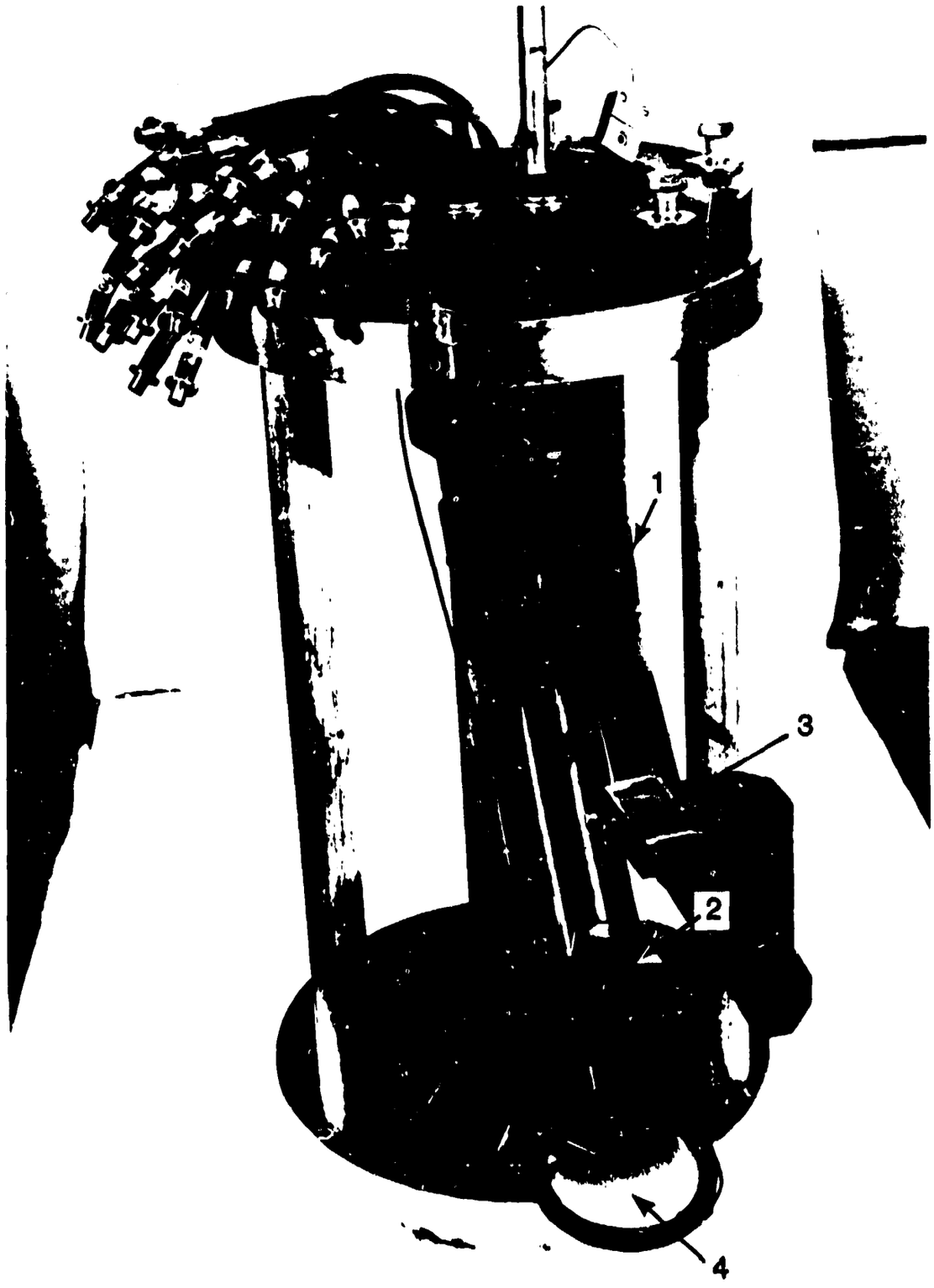

Figure 8. Photograph of the beam mirror system and telescope fastened together, mounted on an external jig.

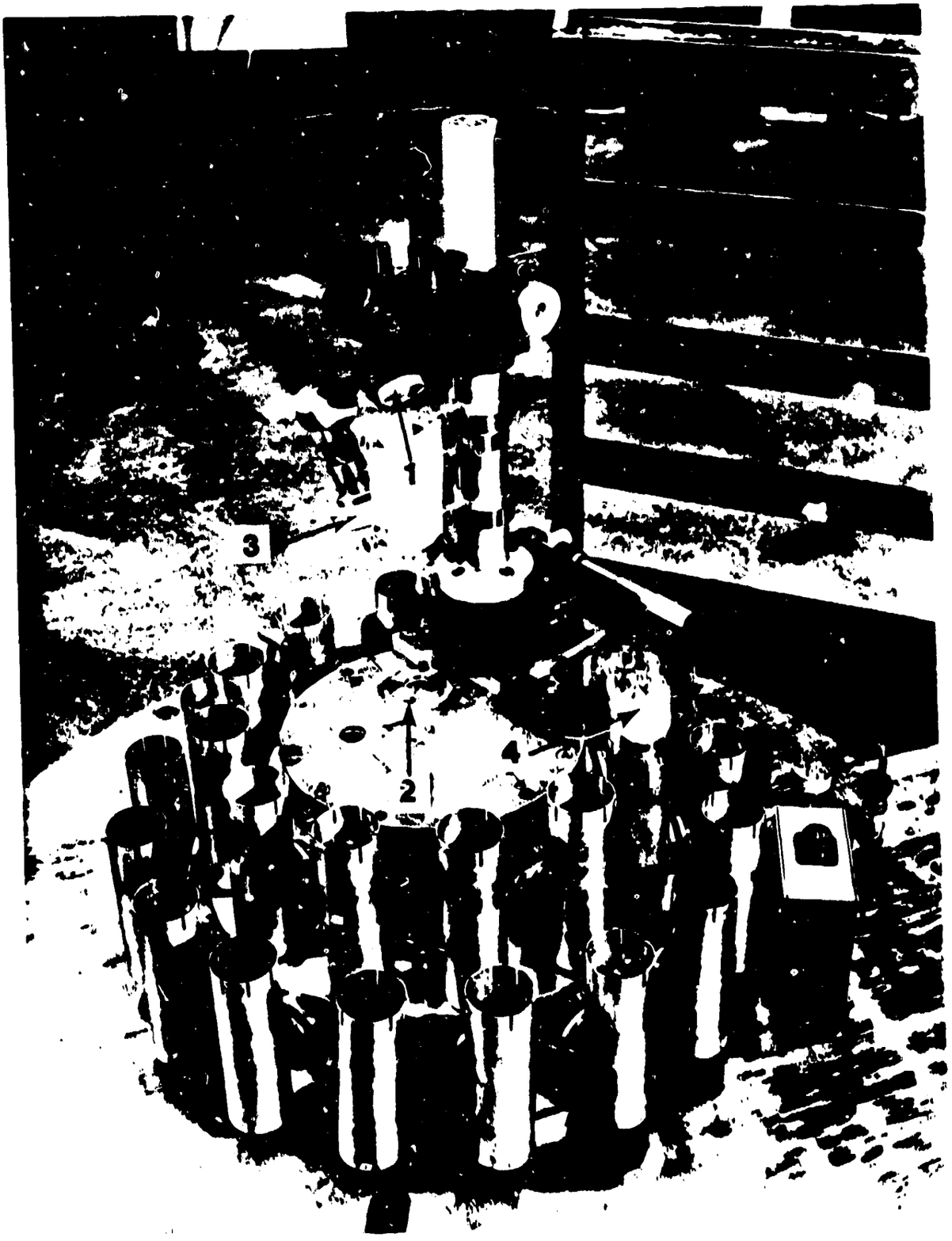

Figure 9. Photograph of the external optical housing.

is used to measure the energy of each laser pulse. The LIF signal light output of each of the 26 fiber bundles is focused through a lens onto the photocathode of a photomultitplier tube (4). Leads from each photomultiplier tube carry the signal from each optical channel to the digital signal processing system.

DIGITAL SAMPLING OF SIGNAL DATA

The phototube current from each optical channel is digitized by a multichannel digitizing system and is stored in a DEC LSI-11 minicomputer for processing, unfolding, and analysis. Signal averaging techniques are used to reduce the effects of signal fluctuations caused by noise and by photon statistical effects. The effects of signal fluctuations on the values of the signal parameters determined from the measurement processes are also determined by subdividing signal samples into subsets to determine mean and standard deviations for intensity and lifetime.

Figure 10 is a schematic diagram that illustrates how a typical LIF optical channel signal output is digitally sampled. The phototube current for the jth optical channel is sampled over K time intervals using charge digitizers to integrate the current over each sampling time interval. The incoming signal is first divided into K equal signals by a matched fanout. Each of the K signals is then fed into one of the charge integrators.* The sampling time of each integrator is controlled by an external gate, controlled by a delay gate generator. The delay gate generator emits a square wave signal of width Δt_k that arrives at the charge digitizer at a time t_k after the laser is fired. The kth charge digitizer samples the photocurrent signal while the gate is "on"; i.e., during the time period t_k to $t_k+\Delta t_k$. Each time the laser is fired the charge digitizer integrates the photocurrent, obtaining a charge value, Q_{jk}, given by

$$Q_{jk} = \int_{t_k}^{t_k+\Delta t_k} dt I_j(t) \quad . \qquad (1)$$

*EG&G QD410 and LeCroy 22495G charge digitizers are presently being used to obtain the signal time samples.

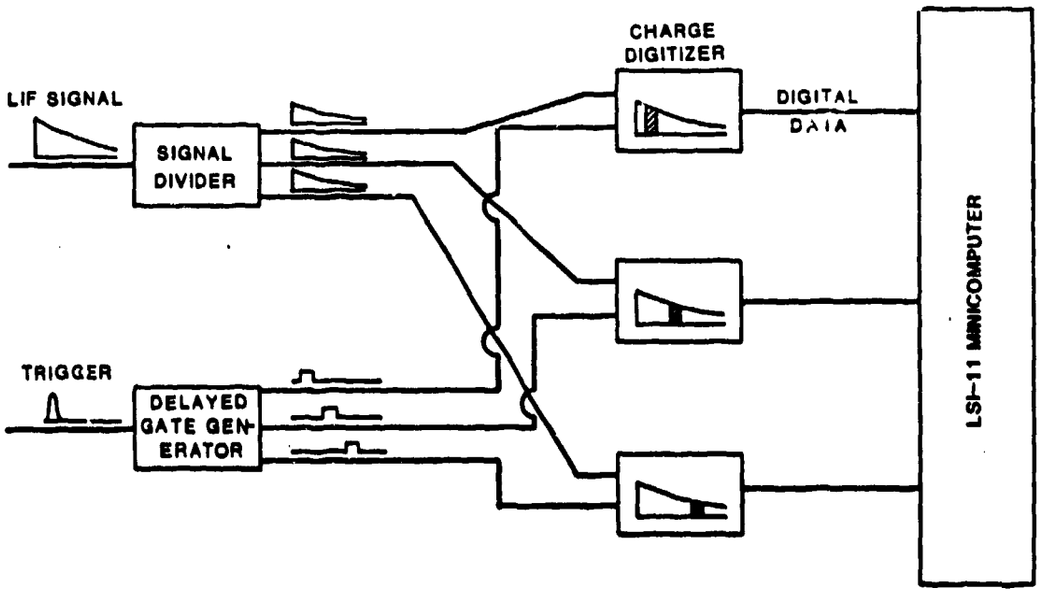

Figure 10. Schematic diagram illustrating how the output from a typical LIF channel is digitally sampled

Another digitizer integrates the output of the photodetector used to monitor the incoming laser pulse. The laser energy per pulse, E_o, is given by

$$E_o = \text{const} \times \int_o^{\Delta t} dt I_m(t) \quad , \tag{2}$$

where Δt is a time interval long compared to the duration of the laser pulse and I_m is the output current of the laser pulse monitor photodetector. Using the value of E_o, one obtains a normalized value of the photocurrent from the jth optical channel, $\tilde{I}_{jk}$, defined by the relation

$$\tilde{I}_{jk} = \frac{1}{E_o \Delta t_k} \int_{t_k}^{t_k + \Delta t_k} dt I_j(t) \quad . \tag{3}$$

Averages can then be obtained by summing the normalized outputs from each charge detector over M laser shots. We obtain,

$$\langle \tilde{I}_{jk} \rangle = \frac{1}{M} \sum_{m=1}^{M} \tilde{I}_{jk} \quad . \tag{4}$$

By obtaining averages over sets of sequences of laser shots, the standard deviations for $\langle \tilde{I}_{jk} \rangle$ can also be obtained.

An attempt is made to obtain signal averaged values for $\langle \tilde{I}_{jk} \rangle$ over 3 to 5 average decay times. At present, the data occuring during the first 3 LIF decay lifetimes is used to make weighted least square fits of the exponential function

$$\tilde{I}_j(t) = \tilde{I}_o^j \, e^{-t/\tau_j} \tag{5}$$

to the sets of data $\{\langle\tilde{I}_{jk}\rangle\}_{k=1}^{K}$, using only those values of $\langle\tilde{I}_{jk}\rangle$ for which $t_k \leq 3\,\tau_j$.*

The gas density and temperature information is contained in the signal intensity and lifetime parameters, $\tilde{I}_o^j$ and τ_j.

*This is done at present to avoid the necessity of applying signal form correction factors to the late time data. (This is discussed in a later section.)

CHARACTERISTICS OF THE LIF SIGNAL

Measurement of the LIF decay lifetime for UF_6 for a number of excitation wavelengths under a variety of gas temperature and pressure conditions have been made by various investigators.[1,3-5,7-10] Of particular interest for our application is the recent work of Rice et al.,[3] who made a careful measurement the temperature dependence of the LIF decay lifetime for an excitation wavelength of 392.1 nm at pressures from 0.005 torr to 85.0 torr. Measurements were made at temperatures in 10°C increments with values ranging from -30°C to 100°C. They developed a simple kinetic model of UF_6 excited state dynamics. A standard kinetic treatment of the model yielded a simple formula that relates the LIF decay lifetime to the UF_6 gas pressure and temperature. They obtained the following expression for the LIF decay lifetime of UF_6:

$$\frac{1}{\tau} = k_u + k_c P + k_1 P \left[\frac{1 + (\alpha+\beta)P}{1 + (\alpha+\beta+\gamma)P + \beta\gamma P^2} \right] , \qquad (6)$$

where P is the gas pressure and k_u, k_c, k_1, α, β and γ are functions of the gas temperature only.

Each of the six coefficients in Eq. (6) was determined by a least squares technique using data obtained from their measurements. The temperature dependence of each coefficient was assumed to satisfy an Arrhenius relationship of the form

$$k = A\, e^{-E/RT} , \qquad (7)$$

where T is the gas temperature and R is the UF_6 gas constant. Values of the parameters obtained by Rice et al. are given in Table I. Equation (6) is

useful for predicting the value of the LIF A_1 state fluorescence decay lifetime given values of the gas pressure and temperature. It can also be used to estimate the rate of variation of the UF_6 A_1 state fluorescence lifetime with changes in gas temperature and pressure.

Table I.

Arrhenius Parameters for UF_6 Self Quenching Rate Constants at 392.1 nm[3]

Rate Constant	A	E/R (K)
k_u	2.30×10^5 s^{-1}	761.6
k_c	1.31×10^8 $torr^{-1}s^{-1}$	2114.
k_l	2.43×10^7 $torr^{-1}s^{-1}$	953.3
α	6.00×10^1 $torr^{-1}$	1693.
β	1.12×10^1 $torr^{-1}$	1731.
γ	2.15×10^{-1} $torr^{-1}$	-260.3

The solid lines in the decay lifetime-pressure plots shown in Figure 2 were obtained using Eq. (6). It can be seen that Eq. (6) gives good estimates of the UF_6 decay lifetime at gas pressures above 0.2 torr.

The jth optical channel of the probe views a small cylindrical fluorescing volume element V_j, located at a radius r_j relative to the axis of rotation of the rotor. V_j is a segment of the cylindrical volume of gas excited by the probe laser beam, which has a radius R_j^b. The volume element, shown in Fig. 11, has a height ΔX_j, given by

$$\Delta X_j = \frac{1}{2} (X_{j+1} - X_{j-1}) \quad , \tag{8}$$

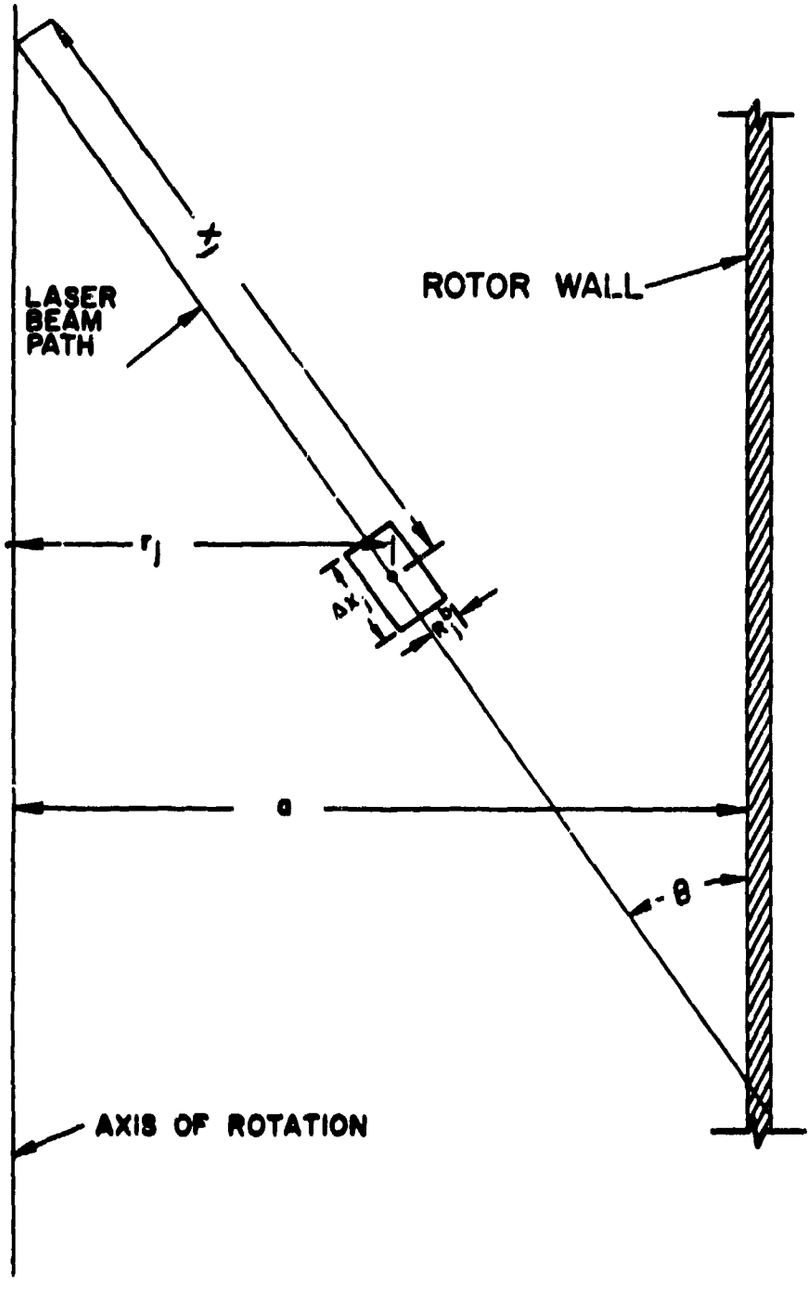

Figure 11. Sketch showing the cylindrical volume element observed by a typical LIF probe optical channel.

where X_j is the distance along the incoming laser beam path to the centroid of V_j from the axis of rotation of the rotor. The total number of UF_6 molecules in the volume element observed by the jth probe channel (N_j) is given by

$$N_j = \pi(R_j^b)^2 \Delta X_j \bar{n}_j = V_j \bar{n}_j \quad , \tag{9}$$

where $\bar{n}_j$ is the average number density of the UF_6 molecules in V_j. When the volume element is excited by a laser pulse of energy E_j, a total of N_p^j fluorescence photons are emitted from V_j, where

$$N_p^j = \frac{\bar{n}_j \sigma_j E_j \Delta X_j Q_F^j}{h\nu} \quad . \tag{10}$$

Here, $\sigma_j = \sigma(\bar{T}_j)$ is the temperature dependent absorption cross section of UF_6 at the average gas temperature of the volume element, $\bar{T}_j$, h is Planck's constant and ν is the frequency of the probe laser. The quantity $Q_F^j = Q_F(\bar{n}_j, \bar{T}_j)$ is the fluorescence quantum efficiency of the UF_6 gas in V_j.

The laser energy arriving at the point of observation (E_j) is given by

$$E_j = E_o T_{io} T_{ig}^j \quad , \tag{11}$$

where T_{io} is the transmission coefficient of the incoming beam optical system. T_{ig}^j is the incoming signal gas attenuation coefficient, given by

$$T_{ig}^j = \int_0^{X_j} dx e^{-n(x)\sigma x} \quad , \tag{12}$$

where the integral is evaluated along the incoming beam path from a point in the inner vacuum core of the rotor to the point of observation.

Generally, T_{ig}^{j} is close to unity (i.e., only a small percentage of the incoming laser energy is absorbed by the gas), and the approximation

$$T_{ig}^{j} \cong e^{-\beta_j \bar{n}_j} \tag{13}$$

is adequate. Here,

$$\beta_j = \sigma_j R \bar{T}_j / \omega^2 r_j \sin\theta \quad , \tag{14}$$

where R is the gas constant for UF_6 and ω is the rotational speed of the rotor.

It can be shown that the photocurrent $I_j(t)$ generated by the jth optical channel is given by

$$I_j(t) = E_o T_{io} \bar{I}_o^j e^{-t/\tau_j} \quad , \tag{15}$$

where $\tau_j = \tau(\bar{n}_j, \bar{T}_j)$ is the average decay lifetime of the gas in V_j. The normalized signal intensity parameter, $\bar{I}_o^j$, is given by

$$\bar{I}_o^j = K_j T_{ig}^{j} \bar{n}_j \chi_j \quad , \tag{16}$$

where

$$\chi_j = \sigma_j Q_F^1 / \tau_j \quad . \tag{17}$$

K_j is determined by calibrating the probe system.*

An analysis of the temperature sensitivity of χ_j has been made using values of Q_F obtained from the work of de Witte et al.[11] with values of σ and τ obtained from the work of Rice et al. Calculations of values of χ at temperatures ranging from 20°C to 60°C indicate that χ_j is only weakly dependent on the gas density and temperature. This means that the normalized signal intensity parameter $\tilde{I}_o^j$ is nearly proportional to the local gas density $\bar{n}_j$ and is nearly independent of the local gas temperature $\bar{T}_j$.

In order to determine the values of $\bar{n}_j$ and $\bar{T}_j$ from the measured values of $\tilde{I}_o^j$ and τ_j, an iteration process may be necessary:

(1) First, values of χ_j and T_{ig}^j are estimated. (Excellent first guesses can be made, because both χ_j and T_{ig}^j are nearly independent of the state of the gas in V_j.)

(2) A value of $\bar{n}_j$ is computed using the known value of $\tilde{I}_o^j$ and Eq. (16).

(3) A value of $\bar{T}_j$ is computed using values of $\bar{n}_j$ and τ_j, either by inverting Eq. (6) or by interpolation of tabular listings of fluorescence lifetime data.

(4) The process is repeated, if necessary, using updated values of χ_j and T_{ig}^j.

*K_j is a product of factors that includes the optical tranmission coefficient of the telescope and optical fiber bundle and the photomultiplier gain.

EFFECTS OF DENSITY STRATIFICATION

When LIF measurements are made in the highly stratified environment of a strongly rotating gas, care must be taken in unfolding the data when the gas density varies appreciably in the radiating volume element V_j. If the dimensions of V_j become comparable to the density scale height, λ_j, then several stratification effects must be taken into account in the data unfolding process:

(1) If R_j^b/λ_j or $\Delta X_j/\lambda_j$ becomes appreciable, then the average gas density in the radiating volume element, $\bar{n}_j$, becomes significantly larger than the gas density at the center of the volume element, $n(r_j)$. For an exponentially varying equilibrium wheel flow atmosphere, it can be shown that

$$\bar{n}_j = n(r_j)\left[1 + \frac{1}{8}\left(\frac{R_j^b}{\lambda_j}\right)^2 \cos^2\theta + \frac{1}{24}\left(\frac{\Delta X_j}{\lambda_j}\right)^2 \sin^2\theta + \ldots\right] \quad . \qquad (18)$$

In our experimental geometry, the dominant term is the first correction term, which involves the ratio of the laser beam radius to the density scale height. If R_j^b/λ_j has a value greater than 0.4 then corrections must be made to $\bar{n}_j$ to obtain the proper value of the gas density at the centroid of the volume element.

(2) When the dimensions of the radiating volume element become comparable to the density scale height, the time variation of the signal will begin to deviate measurably from the classical exponential shape. The reason for this is that in cases where density variations are large in the radiating volume element, a significant fraction of the volume element has a decay lifetime that is appreciably different from the mean decay time.

Low density regions have a decay lifetime that is longer than the mean. As a result, after several decay times, the population of excited states in the low-density regions will be higher than the average value and will begin to dominate the signal. At late times, then, the total signal amplitude will be higher than the value characteristic of a single exponential decay at the average fluorescence decay rate. If there are significant gas density variations in V_j, then the photocurrent signal $I_j(t)$ is given by a generalization of Eqs. (15) and (16):

$$I_j(t) = K_j E_o T_{io} \int_{V_j} dv\, T_{ig}(\vec{r}) \frac{\sigma Q_F(\vec{r})}{\tau(\vec{r})} e^{-t/\tau(\vec{r})}\, n(\vec{r}) \quad . \tag{19}$$

It can be shown that the signal $I_j(t)$ can be represented by the functional form

$$I_j(t) = E_o T_{io} \bar{I}_o^j e^{-t/\tau_j} f(t) \quad , \tag{20}$$

where the correction time function, f(t) has the general behavior

f(t) is close to unity if $t/\tau_j \lesssim 1.0$

$f(t) > 1.0$ if $t/\tau_j > 1.0$.

Computer calculations of f(t) have been made using the equilibrium solid body rotation gas density profile. Results of these calculations, obtained for values of $R_j^b/\lambda_j \leq 0.3$ and $0.3 < \Delta X_j/\lambda_j < 0.4$* show that:

*These are typical values expected in our experiments.

(1)	if $t/\tau_j < 2.0$	f(t) is essentially unity
(2)	if $t/\tau_j = 3.0$	$1.02 \leq f(t) \leq 1.03$
(3)	if $t/\tau_j = 4.0$	$1.05 \leq f(t) \leq 1.09$
(4)	if $t/\tau_j = 5.0$	$1.08 \leq f(t) \leq 1.16$ (21)

From these calculations, we have concluded that signal shape correction factors must be applied to values of $I_j(t)$ at times greater than three average decay times before attempts are made to fit simple time exponential shape factors to obtain values of $\tilde{I}_o^j$ and τ_j. At present, data is being used during the first three average decay times to determine $\tilde{I}_o^j$ and τ_j, as uncertainties in the proper values of f(t) are small in this time range.

SIGNAL SAMPLING PERIODS AND PHOTON STATISTICS

The primary cause of signal fluctuations is random variations in the number of photons entering the telescope aperture. The choice of signal sampling periods must be chosen to minimize the uncertainty in the least squares fit of $\tilde{I}_o^j$ and τ_j. The number of fluorescence photons expected to be received in optical channel j during sample period k ($\hat{N}_{jk}$) is given by

$$\hat{N}_{jk} \propto \int_{t_k}^{t_k+\Delta t_k} I_o^j \, e^{-s/\tau_j} \, ds = I_o^j \tau_j f_{jk} \quad , \tag{22}$$

where

$$f_{jk} = \left(e^{-t_k/\tau_j} - e^{-(t_k+\Delta t_k)/\tau_j}\right) \tag{23}$$

In order to obtain good fits for $\tilde{I}_o^j$ and τ_j, the sampling time periods for each optical channel must be chosen to be consistent with the values of signal decay times expected to occur. Sample times are chosen using the following assumptions and limitations:

(1) Maximum number of samples per optical channel is limited ($\lesssim 10$)

(2) All samples must be taken during the first three decay times, because the signal deviates significantly from a pure exponential at later times.

(3) Poisson statistics apply.

A statistical analysis based on the above assumptions results in the following criteria for sample time selection:

(1) Sample intervals should be contiguous ($t_{k+1} = t_k + \Delta t_k$) and extend from t = 30 ns to $t = 3\tau_j$.*

(2) 8-10 samples per optical channel is about optimum.

(3) The expected number of photons detected during each sampling period should be essentially identical.

As noted in Eq. (22), the number of photons sampled is proportional to $\tilde{I}_o^j$ and τ_j. $\tilde{I}_o^j$ is very nearly proportional to the average molecular number density, $\bar{n}_j$. Since the decay lifetime <u>increases</u> as the number density <u>decreases</u>, the number of photons detected in each sampling period will decrease quite slowly with gas density, if the signal sampling periods are allowed to increase in proportion to the signal decay time. Consider an isothermal gas in solid body rotation. The ratio of the number of photons detected during a sampling period at two gas pressures P_1 and P_2, $R(P_1, P_2)$, is given by

$$R(P_1,P_2) = \frac{\hat{N}_{jk}(P_1)}{\hat{N}_{jk}(P_2)} \cong \frac{P_1\tau_1 f_{1k}}{P_2\tau_2 f_{2k}} \quad . \tag{24}$$

The number of photons detected per time sample drops relatively slowly with gas density if values of f_{jk} are held fixed in all channels. This is illustrated by values of $R(P_1, 100\ \text{torr})$, given in Table II for various values of the gas pressure. Here, we give the ratio of $\hat{N}_{jk}$ at a gas pressure of 100 torr. Values shown are calculated for a gas temperature of 20°C.

*Actually, results can be improved by extending the sample period beyond $3\tau_j$ if the correction function f(t) is well known.

TABLE II.

Variations in the Relative Numbers of Photons Detected in a Signal Sampling Period*

P_1(Torr)	τ(ns)	$R(P_1, 100)$ $\Delta t_k/\tau_j$ = const.	$R(P_1, 100)$ Δt_k = const.
100	54	1.0	1.0
10	2.5×10^2	0.46	10^{-1}
1	1.3×10^3	0.24	10^{-2}
0.1	8.8×10^3	0.16	10^{-3}
0.01	3.6×10^4	0.066	10^{-4}

*Lifetime values shown are for a gas temperature of 20°C.

Average lifetimes at pressures ranging from 100 torr to 10^{-2} torr are shown in column 2. Changes in the relative number of photons detected during a sampling period, expressed as a fraction of the value at a pressure of 100 torr, are shown in column 3 for the case where $\Delta t_k/\tau_j$ is held fixed. Note that the number of photons detected drops only by a factor of 15 when the pressure drops by four orders of magnitude. If the signal sampling time period is kept at a fixed value as the lifetime increases, then the situation is quite different. In this case, $\hat{N}_{jk} \alpha P$, and the number of photons sampled during Δt_k drops rapidly with gas pressure. This is illustrated in column 4. From these results we see that it is necessary to utilize an electronic digitizing system that is capable of covering a very wide range of signal sampling times in order to obtain the best results with minimum

photon fluctuation effects. Signal sampling times must vary from intervals of approximately 20 ns to 20 μs. Gate delay times must vary from 20 ns to 150 μs, in order to optimally sample LIF signals in the pressure range given in Table II.

INTERPRETATION OF SIGNAL PARAMETER VARIATIONS

The signal variables obtained directly from the probe output are $\tilde{I}_o^j$ and τ_j. Of interest to us, however, are $\bar{n}_j$ and $\bar{T}_j$. A valuable aid in relating signal parameter variations to gasdynamic variable changes can be obtained by obtaining relationships for fractional changes in variables. Define small changes in the signal parameters and the gas dynamic variables by δ. Then, we can differentiate Eqs. (6) and (16) to obtain

$$\frac{\delta\bar{I}_o}{\bar{I}_o} = I_n \frac{\delta\bar{n}}{\bar{n}} + I_T \frac{\delta\bar{T}}{\bar{T}} \quad , \tag{25}$$

$$\frac{\delta\tau}{\tau} = \tau_n \frac{\delta\bar{n}}{\bar{n}} + \tau_T \frac{\delta\bar{T}}{\bar{T}} \quad , \tag{26}$$

where

$$I_n = 1 + \frac{\bar{n}}{T_{ig}} \frac{\partial T_{ig}}{\partial \bar{n}} + \frac{\bar{n}}{\chi} \frac{\partial \chi}{\partial \bar{n}} \quad , \tag{27}$$

$$I_T = \frac{\bar{T}}{T_{ig}} \frac{\partial T_{ig}}{\partial \bar{T}} + \frac{\bar{T}}{\chi} \frac{\partial \chi}{\partial \bar{T}} \quad , \tag{28}$$

$$\tau_n = \frac{\bar{n}}{\tau} \frac{\partial \tau}{\partial \bar{n}} \quad , \tag{29}$$

$$T_\tau = \frac{\bar{T}}{\tau} \frac{\delta\tau}{\delta\bar{T}} \quad . \tag{30}$$

We can solve equations (25) and (26) to obtain expressions for fractional density and temperature variations, obtaining

$$\frac{\delta\bar{n}}{\bar{n}} = n_I \frac{\delta\tilde{I}_o}{\tilde{I}_o} + n_\tau \frac{\delta\tau}{\tau} \tag{31}$$

$$\frac{\delta\bar{T}}{\bar{T}} = T_I \frac{\delta\tilde{I}_o}{\tilde{I}_o} + T_\tau \frac{\delta\tau}{\tau} \ , \tag{32}$$

where

$$n_I = \frac{\tau_T}{I_n\tau_T - I_T\tau_n} \ , \tag{33}$$

$$n_\tau = \frac{-I_T}{I_n\tau_T - I_T\tau_n} \ , \tag{34}$$

$$T_I = \frac{-\tau_n}{I_n\tau_T - I_T\tau_n} \ , \tag{35}$$

$$T_\tau = \frac{I_n}{I_n\tau_T - I_T\tau_n} \ . \tag{36}$$

Equations (31) and (32) are very useful for determining the differences in gas conditions in gas volumes viewed by adjacent optical channels. Values of $\delta\tilde{I}_o$ and $\delta\tau$ can be obtained by differencing values of $\tilde{I}_o^j$ and τ^j in adjacent optical channels. Values of $\delta\bar{n}$ and $\delta\bar{T}$ can then be obtained by calculation, using equations (31) and (32).

Simplified forms of equations (31) and (32) are also very useful for interpreting changes in local gas conditions from changes in observed LIF

signals. The dominant nature of these relationships can be determined by noting that to a very good approximation, $\tilde{I}_o^j \alpha n_j$, and

$$I_n = n_I \cong 1.0 \tag{37}$$

$$I_T = n_\tau \cong 0 \tag{38}$$

Then, in this approximation,

$$\frac{\delta \bar{n}}{\bar{n}} = \frac{\delta \tilde{I}_o}{\tilde{I}_o} \quad , \tag{39}$$

$$T_I = - \tau_n / \tau_T \quad , \tag{40}$$

and

$$T_\tau = 1/\tau_T \quad . \tag{41}$$

Values of T_I and T_τ have been obtained by differentiating Eq. (6). Curves of T_I and T_τ vs gas pressure are plotted in Figures 12 and 13 for three values of gas temperature, 20°C, 40°C, and 60°C. It can be seen that T_I and T_τ do not vary strongly with gas temperature or pressure, although the decay lifetime and quantum efficiency are both strong functions of gas pressure.

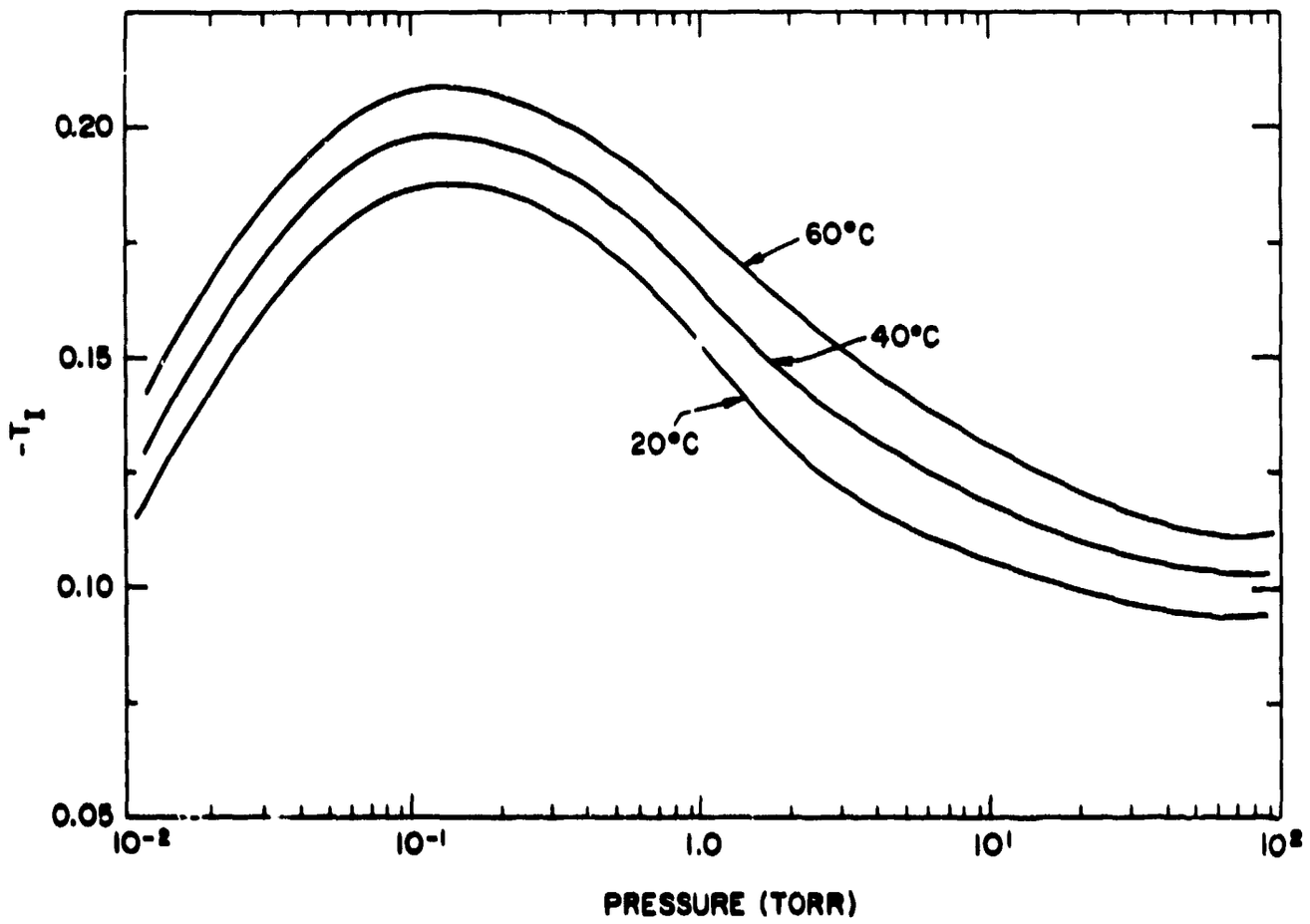

Figure 12. Variation of T_I with gas pressure at temperatures of 20° C, 40° C and 60° C

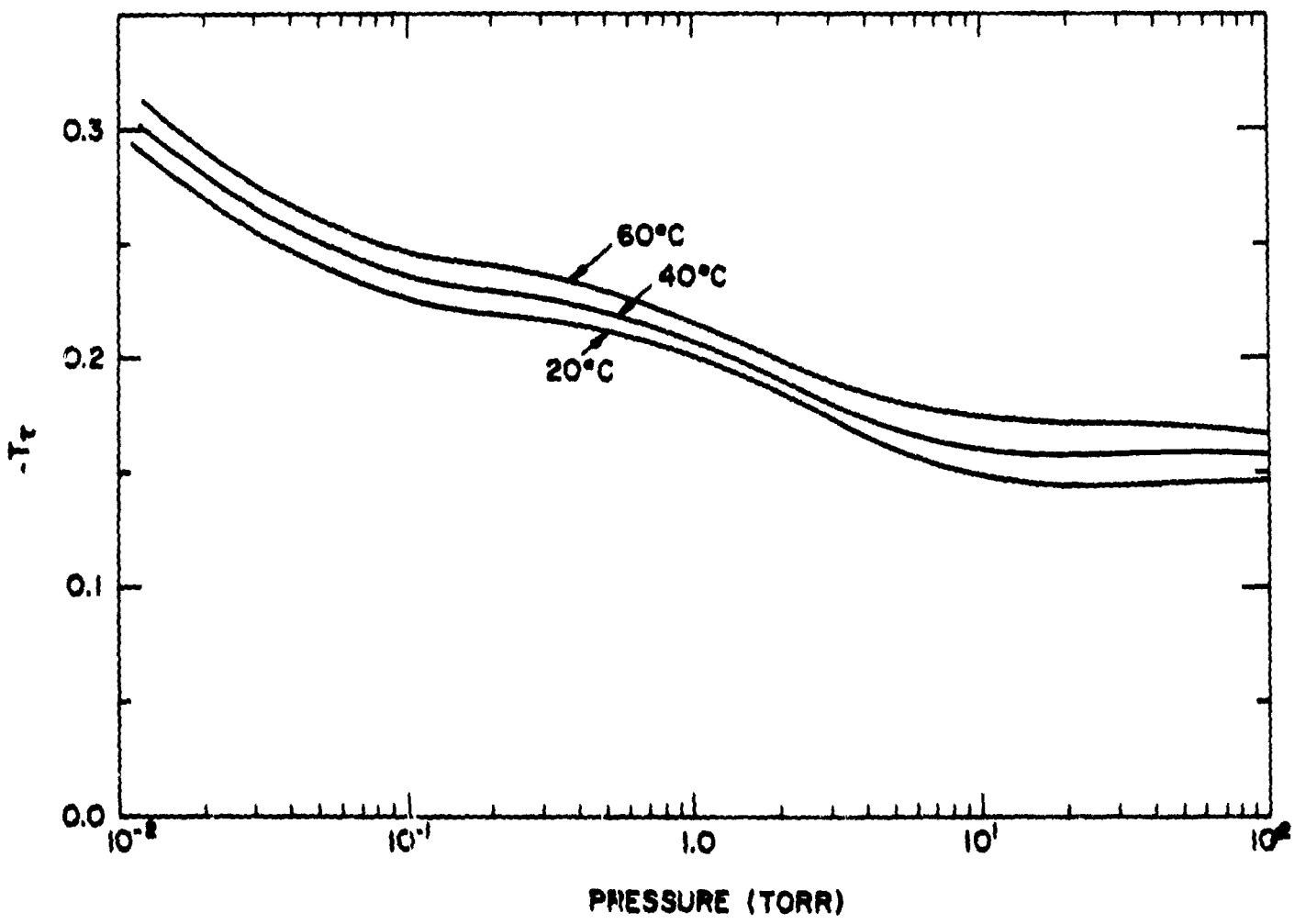

Figure 13. Variation of T_T with gas pressure at temperatures of 20° C, 40° C and 60° C.

EFFECTS OF LASER EXCITATION ON THE GAS

When the gas is excited by a laser pulse, some fraction (ψ_j) of the UF_6 molecules in the volume element V_j will be excited, where,

$$\psi_j = \frac{E_j \sigma_j}{h\nu A_j} \quad . \tag{42}$$

Here, A_j is the laser beam cross-sectional area in V_j. Typically, $E_j \approx 1$ mj and $A_j \approx 0.03$ cm^2. Thus,

$$\psi_j \approx 10^{-3} \quad ;$$

i.e., only a small fraction of the gas molecules are excited by a single laser pulse. A large fraction of the excited molecules will dissociate, forming UF_5 and F. Thus, the immediate effect of the absorption of laser energy will be to slightly reduce the number density of UF_6. The absorption of laser energy can also change the gas temperature slightly. However, since only an extremely small percentage of the gas interacts with the laser beam, beam excitation effects on the state of the gas are negligible as long as beam diameters are on the order of a few mm and laser pulse energies are on the order of 1 mj.

REMOVAL OF EXTRANEOUS SIGNALS

The raw signals produced by each photomultiplier tube contain several extraneous effects that must be either removed or corrected for:

1. Background signals. The system continously monitors the background signals by making background signal measurements between laser pulses. Average background signals are subtracted from the raw signals produced by the probe.

2. The probe laser produces intense amounts of scattered light in the interior of the rotor that can enter the telescope. Since the direct laser signal thus produced is far more intense than the fluorescence signal received by the telescope, it must be removed before a good analysis of the fluorescence signal can be made. Probe laser light effects are removed by a combination of methods:

   a. Two filters are placed in series in the probe telescope that filter out most of the light entering the telescope with a wavelength below 400 nm.

   b. Signal data is not recorded for times earlier than about 30 ns, when large amounts of laser optical energy are detected by the photomultiplier tubes.

   c. Measurements of the average scattered laser light received by the probe at times later than 30 ns in the absence of gas in the rotor are made by operating the probe in an empty rotor and recording the average signal amplitudes in each optical channel during the sampling times. These "zero gas" signals, which are generally very small at times later than 30 ns, are also subtracted from the raw signal.

CALIBRATION PROCEDURES FOR THE LIF PROBE

Two types of calibration procedures must be performed on the assembled probe system in order to make full use of the information content of the LIF signal. To make them, the probe is pre-assembled outside the rotor in an alignment jig that holds the top cover of the rotor casing. The optical components of the probe have been designed so that they can be disassembled after calibration and reassembled during installation in the rotor without materially changing the orientation of the probe optics relative to the axis of rotation. This permits the orientation of the optical system relative to the axis of rotation to be accurately determined.

The first calibration process involves mapping the field of view of each optical fiber channel. After the probe is assembled and the incoming beam mirrors are adjusted, a small diameter ($\sim$0.1 mm) standard intensity light source is mounted on a micrometer translating system and is moved along the incoming beam path in a controlled manner. By measuring the displacement of the light source along the light path and observing the onset and extinguishment of the light signal in the jth optical fiber channel, values of X_j and ΔX_j can be determined. By observing signal intensities generated by each optical fiber channel, channel-to-channel variations in transmission coefficients can also be obtained.

In order to utilize the signal intensity data, the quantity K_j must also be known. This is done by mounting a windowed gas cell containing UF_6 gas at a known gas pressure and temperature in the laser beam path. The laser probe system is operated with the gas cell producing

an LIF signal. Values of signal intensity and lifetime can be determined in each optical channel, and values of K_j can be determined from the calibration test data. In order to obtain accurate values of K_j, it is necessary to correct values of signal intensities obtained during calibration tests in the gas cell for slightly different incoming laser beam attenuation occurring in the gas cell. (That is, T_{ig}^{j} has a slightly different value in the gas cell than it does in the rotor during actual operation.)

DETERMINATION OF THE LOCATION OF EACH POINT OF MEASUREMENT WITH RESPECT TO THE ROTOR WALL

In order to properly interpret the gas density and temperature data in the rotating gas layer, it is necessary to determine the radial distance of each radiating volume element from the inner wall of the rotor at operating speed. This can be done by varying the radial location of the field of view of the telescope and observing the variations in the signal intensity of those probe channels that view the rotating gas in the vicinity of the rotor inner wall. As the field of view of a given optical channel is moved outward radially through the gas layer, the signal intensity will initially increase as the gas density increases. However, a point is eventually reached where the signal intensity no longer increases, as part of the radiating volume element viewed is excited by the laser beam that is reflected from the rotor wall, rather than by the incoming, unreflected laser beam. Thus, there is a point at which a given optical channel will produce a maximum intensity. Maximum intensity occurs when the centroid of the optical channel is slightly inboard from the rotor wall. If the relative locations of the centroids of each optical channel have been previously determined by a mapping procedure, the locations of each channel relative to the rotor wall are determined once the location of a single channel is determined.

EXPERIMENTAL RESULTS

The LIF probe has been assembled and operated in a small laboratory rotor containing UF_6 gas, and the probe has been used to measure the radial distribution of the fluorescence lifetimes in the interior. In this test, the LIF probe was operated with a single active photomultiplier tube, permitting the measurement of the fluorescence lifetime at a single point at a given time. A radial distribution of LIF lifetimes was obtained by moving the single active photomultiplier from one fiber optics channel to another, obtaining lifetime data at various radial locations over an extended period of time.

At the beginning of an experiment, the rotor was filled with gas and was allowed to run for some time to establish thermal equillibrium before the LIF lifetime measurements were made. A small scoop was left at a point high in the gas atmosphere, where scoop pressures on the order of 0.5 torr were produced. By monitoring the value of the scoop pressure at a fixed radial position, an approximate value of the relative rotor gas inventory could be determined during the course of an experiment. The external rotor temperature was determined using calibrated pyrometers. Examination of the scoop pressure and rotor temperature data showed that the rotor could be operated for relatively long periods of time with very low rotor inventory losses and with rotor temperature variations on the order of $\pm 2.5°$ C.

LIF signal intensity and lifetime data were obtained from 18 of the 26 optical channels. The LIF decay lifetimes have been used to determine the radial gas pressure distribution of the rotor. Figure 14 depicts the scaled radial pressure distribution obtained from our experiment. Depicted here is the scaled pressure, expressed as a fraction

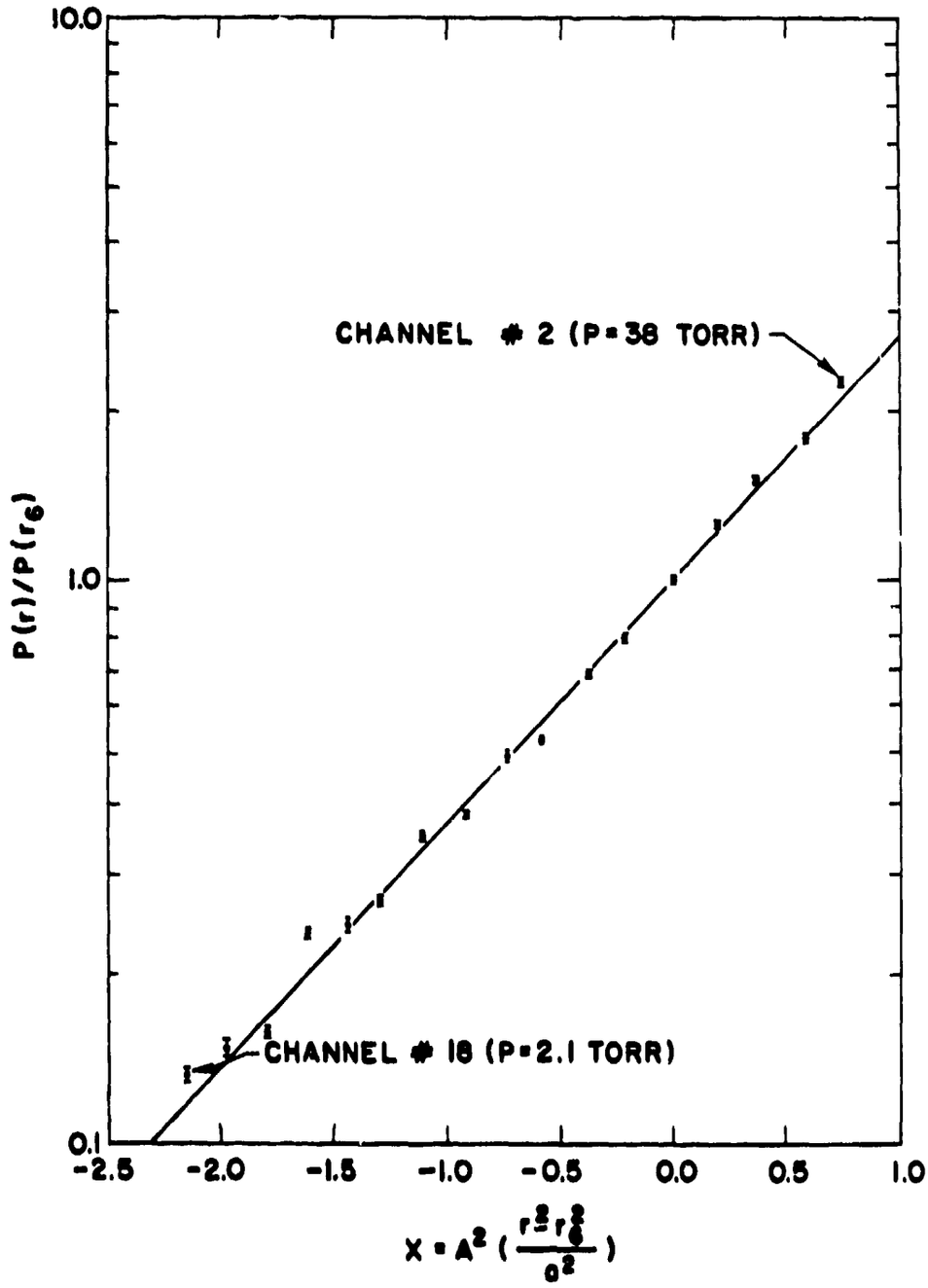

Figure 14. Radial static pressure distribution determined from UF_6 lifetime data. Shown here is a plot of the ratio of the static gas pressure at a radius (r) to the static gas pressure at channel #6, plotted vs the scaled radial variable X

of the pressure in channel #6, plotted as a function of the scaled radial position relative to the radius of channel #6. Here, the scaled radius, X, is given by

$$X = A^2 \left(\frac{r^2 - r_6^2}{a^2} \right) , \qquad (43)$$

where A^2 is the stratification parameter given by the expression

$$A^2 = \omega^2 a^2 / 2R\bar{T}. \qquad (44)$$

The solid line is the pressure variation expected when the gas is in equilibrium solid body rotation. Results of observations shown here represent data taken over a period of time, during which both the STR rotor temperature and gas inventory varied slightly. In order to correct the data for small variations in temperature and speed, the lifetime data has been corrected as follows:

1. All measured lifetimes were first corrected for temperature variations to correspond to a temperature of 314 K, close to the average value of the rotor temperature during the test period.
2. Gas pressures were then determined using equation 6, using an assumed gas temperature of 314 K.
3. Scaled radii (X) values were then calculated using variable values of the stratification parameter (A^2) corresponding to rotor speed and rotor temperature values occurring during the measurement period.

Each data point shown in Figure 14, has been determined from a set of 1,920 laser pulses. Each data set is divided into 10 subsets of lifetime and intensity averages, each representing a sample over 192 laser pulses. The mean and standard deviation of the LIF lifetime have

been calculated for each data point. The estimated standard deviations in the observed gas pressure due to fluctuations in measured LIF signals, calculated from lifetime standard deviations, is shown for each data point. As expected, the standard deviations are smaller at larger radii, where signal intensities are higher. The lifetime standard deviations range from 1% at pressures above 10 torr to 2% to 3% at pressures of 2 to 3 torr. The increase in the fluctuation in the measured lifetimes shown here can be reduced in future experiments. At the time these measurements were made, the signal sampling period (Δt_k) was fixed for all channels at a value of about 27 nsec. This value is optimum for use in sampling LIF signals with decay lifetimes with a value of approximately 80 nsec. At the lower pressures, the sampling period was too short to permit sampling an optimal number of LIF photons. Thus, the photon statistics were not as good as could be achieved by utilizing higher values of Δt_k to sample signals at the lower gas pressures.

Values of pressures calculated from measured lifetimes varied from 38 torr in channel #2 to 2.1 torr at channel #18.

It can be seen that the calculated values of the pressure ratios, determined from measured lifetimes, follow the expected solid body rotation profile quite well in most regions. However, the variation of the pressure ratios determined from lifetimes definitely vary from the solid body rotational flow values by more than the standard deviations in some regions, particularly at low pressure. The error bars shown here include

only the effects of fluctuations in lifetime measurements. There may be errors related to the assumption that the local average gas temperature is equal to the average rotor temperatures.

Figure 15 shows the variation of the average normalized LIF signal intensity in channel #6 with time after laser firing. Each data point shown here is the average signal amplitude, determined from 10 sets of 192 laser pulses. Shown also at each point is the standard deviation. The average decay lifetime determined from this set of data is 118.6 ± 0.9 nsec. At an estimated gas temperature of 312°K, this lifetime yields a calculated gas pressure of 16 torr. The straight line is the least squares fit for an exponential signal shape, obtained using average amplitude data points taken at times less than 350 nsec (3 decay lifetimes). Note that the lifetime amplitude data at times beyond 350 nsec is consistently above the least squares exponential fit. Part of this is due to the effects of stratification in the radiating volume element, mentioned earlier. However, the deviations are larger than our theoretical estimates predict. Either the actual values of R_j^b/λ_j and $\Delta X_j/\lambda_j$ are larger than our estimates, or another effect is present.

Mean values and standard deviations for the signal intensity parameters, $\bar{I}_o^j$, were also calculated from the signal data collected for each channel. It is not possible to utilize the intensity data to determine the gas state, as no calibrations were made prior to performing the experiment reported here. However, the statistical quality of the signal amplitude data has been studied. The standard deviations

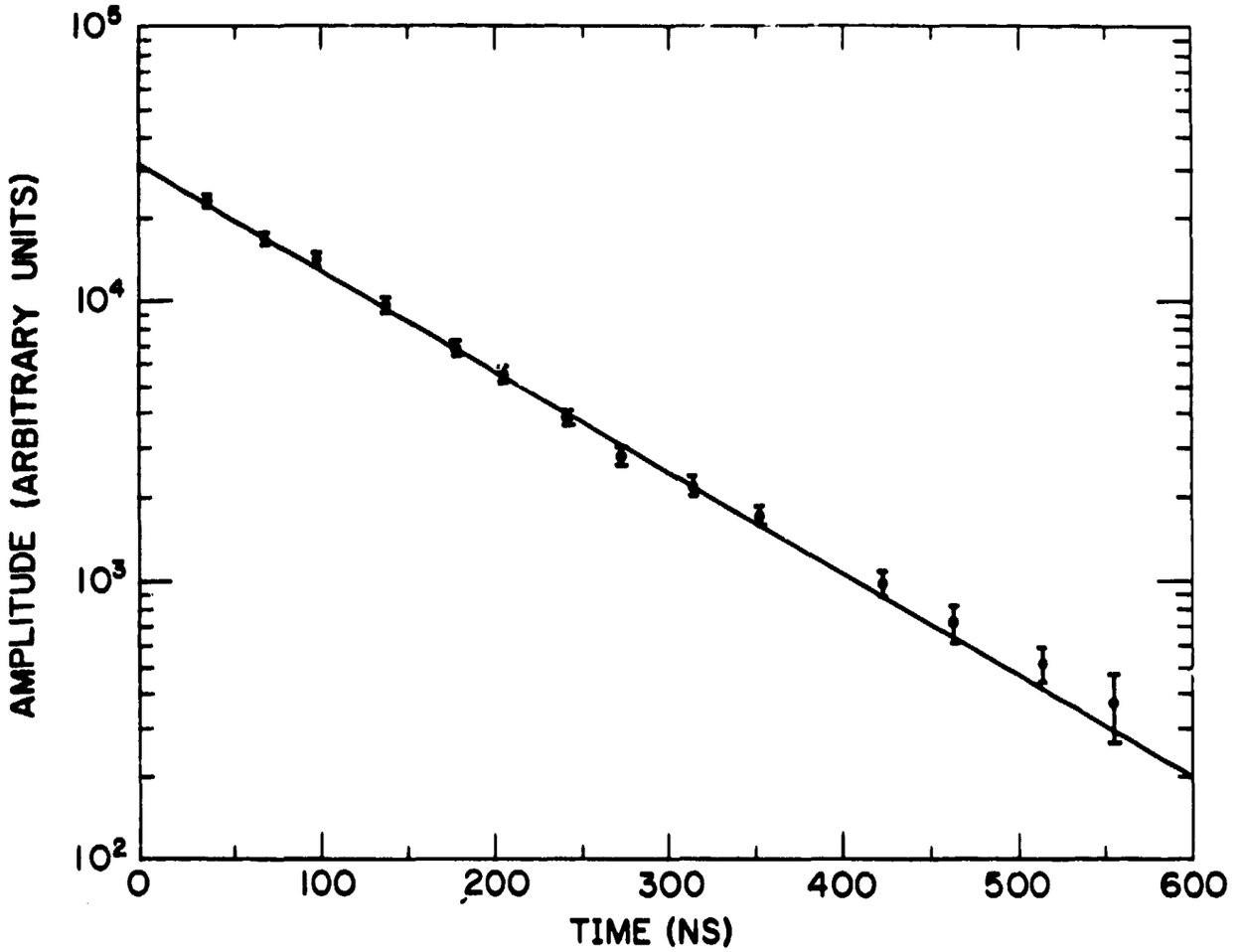

Figure 15. Plot of average LIF signal amplitude vs time. Each data point is an average of 10 sets of data, each set consisting of an average taken over 192 laser pulses. The average decay lifetime determined from this set is 118.6 ± 0.9 nsec.

for $\tilde{I}_o^{\gamma j}$, expressed as fractions of the mean, were about three times the values obtained for the decay lifetimes. It was noted that there were non-random variations in the average values of $\tilde{I}_o^{\gamma j}$ obtained during the measurement period (usually about 30 minutes). Generally, there was a slow decrease in the average amplitude of $\tilde{I}_o^{\gamma j}$ with time. The cause of this apparent drift is not known at the time of this writing.

CONCLUDING REMARKS

The preliminary tests of the prototype LIF probe have demonstrated the feasability of making point measurements of decay lifetimes in the highly stratified environment characteristic of a gas centrifuge. Further development work is in progress. The digital signal processing system has been expanded to permit the collection and analysis of data in six optical channels simultaneously. The digitizing system has been modified to permit variable signal integrating times as long as several hundred ns. A temperature controlled gas cell has been constructed to permit extensive testing of the probe system in a controlled, measured gas environment as well as in a test rotor. Probe performance tests are being carried out in the gas cell:

1. To obtain good calibration data for each optical channel.
2. To further investigate the temperature and pressure dependence of the amplitude factor χ_j, to determine whether accurate evaluations of gas density require small corrections in the amplitude-gas density relationship.
3. To obtain better decay lifetime data at lower pressures.

The analysis presented in earlier sections indicates that the number of photons detected by the probe falls very slowly as the gas pressure drops, if the signal sampling time lengthens with the decay lifetime. Thus, there is a good possibility that the probe system will permit good measurements to be made at low ($\lesssim$0.1 torr gas pressures. However, near term work will be centered on obtaining good measurements at the higher pressures, as the present probe electronics system is not capable of

sampling signals over the long time periods ($\sim 10^4$ nsec) necessary to reduce the effects of photon fluctuations at low pressures. Also, it will be necessary to obtain better lifetime data at low pressures to permit accurate unfolding of LIF signals.

ACKNOWLEDGMENT

This work was performed under the auspices of the United States Department of Energy.

REFERENCES

1. S. De Silvestri, O. Svelto, and F. Zaraga, Appl. Phys. 21, 1 (1980).

2. R. J. Jensen and C. P. Robinson, Laser Focus, 16, (4), 54 (1980).

3. W. W. Rice, R. C. Oldenborg, P. J. Wantuck, J. J. Tiee, and F. B. Wampler, J. Chem. Phys. 73, 3560 (1980).

4. R. C. Oldenborg, W. W. Rice, and F. B. Wampler, J. Chem. Phys. 69, 2181 (1978).

5. P. Benetti, R. Cubbedu, C. A. Sacchi, O. Svelto, and F. Zaraga, Chem. Phys. Lett. 40, 240 (1976).

6. The authors wish to express their thanks to W. Rice for making available here the original data obtained in the lifetime measurements described in Reference 3 above.

7. O. de Witte, R. Dumanchin, M. Michen, and J. Chatelet, Chem. Phys. Lett. 48, 505 (1977).

8. W. B. Lewis, L. B. Asprey, L. H. Jones, R. S. McDowell, S. W. Rabideau, A. H. Zeltmann, and R. T. Paine, J. Chem. Phys. 65, 2707 (1976).

9. A. Andreoni and H. Bucher, Chem. Phys. Lett. 40, 237 (1976).

10. F. B. Wampler, R. C. Oldenborg, and W. W. Rice, Chem. Phys. Lett. 54, 554 (1978).

11. O. De Witte, R. Dumanchin, J. P. Gauyacq, and M. M. Michon. "Laser Induced Processes in Molecules," K. L. Compa and S. D. Smith, eds., 6, 49, Springer Verlag, Berlin (1979).